Path-integral calculation of the two-dimensional ^{4}He phase diagram

M. C. Gordillo and D. M. Ceperley
National Center for Supercomputing Applications and Department of Physics, University of Illinois at Urbana-Champaign, 405 N. Mathews Avenue, Urbana, Illinois 61801

(Received 26 February 1998)

Path-integral Monte Carlo simulations have been used to determine the phase diagram of a two-dimensional ^{4}He film in a range of temperatures and coverages where it undergoes solidification, superfluidity, and a liquid-gas transition ($0.25\ \mathrm{K} \leqslant T \leqslant 1.5\ \mathrm{K}$ $0 < \sigma < 0.094\ \text{Å}^{-2}$). We determine the phase-transition densities and give the coefficients for a functional form of the free energy in the liquid, solid, and gas phases. The phase diagram is similar to the one determined from experimental measurements of a second layer of helium on graphite. [S0163-1829(98)04634-7]

The onset of superfluidity in two-dimensional (2D) films has been the object of much work both experimentally and theoretically. In contrast to bulk helium, the superfluid-normal fluid transition in 2D ^{4}He films is of the Kosterlitz-Thouless type, with superfluidity appearing below the critical temperature, T_c,[1] but with Bose condensation appearing only at $T=0$. Experimental data allows us to delimit the superfluid region,[7–12] and to establish the stability boundaries between solid, liquid, and gas 2D phases[2–6] on substrates such as graphite (bare or preplated).

When the interaction potential between the helium atoms and the absorbing surface is strong (He-graphite, He-H_2) helium atoms are adsorbed in well-defined layers.[13–15] In graphite, one can have up to seven of such layers; additional amounts of ^{4}He lead to the formation of a bulk liquid. Obviously, the first layer is one the most influenced by the adsorbate, while the second layer is very well approximated by a pure 2D film.[10]

By means of calorimetric measurements[2–5] several facts can be established about the 2D phase diagram of ^{4}He. There have been many experiments with the second and third layers of helium adsorbed on graphite, or first layers of He on a H_2 surface. These show a liquid-gas coexistence at low temperature ($\sim$0.75–0.9 K and below). In the case of a second layer of He on graphite, they also agree in the high coverage stability limit of the liquid phase ($\sigma \sim 0.07\ \text{Å}^{-2}$). A solid layer forms at a higher helium density. This region continues until the beginning of the formation of the third layer ($\sigma \sim 0.08\ \text{Å}^{-2}$). There is also a line of specific-heat maxima between 0.0425 and 0.07 Å^{-2} at temperatures lower than 1 K.[2–4] The origin of that line has not received a clear interpretation.

The location of the boundary that separates the superfluid and normal phases has been delineated by torsional oscillator experiments.[16,7,8,10–12] The work of Crowell and Reppy[8–10] indicates a superfluid phase in a range of coverages between 0.05 and 0.07 Å^{-2} at temperatures below 1 K for a second layer of ^{4}He adsorbed on graphite.

On the other hand, most of the theoretical work on 2D helium films has been made for $T=0$ K. Whitlock, Chester, and Kalos,[17] by means of Green-function Monte Carlo (GFMC) calculations, showed that there was a self-bound liquid at a coverage of approximately 0.04 Å^{-2}. For lower densities, there would be a gas-liquid coexistence. The intersection between the curves of the energy versus temperature of the solid and liquid phases gives a lower stability boundary for a 2D solid of about 0.067 Å^{-2}. The results given by Giorgini *et al.*,[18] with a slightly different potential and obtained by a diffusion Monte Carlo (DMC), confirm the above conclusions. The same can be said of the hypernetted-chain calculations of Um *et al.*[19] There are also calculations with a 3D model at $T=0$ K (Refs. 20,21) (substrate+two frozen helium layers), but they produce phase limits very similar to pure 2D calculations. The path-integral Monte Carlo (PIMC) calculations of Ceperley and Pollock[1] take into account the thermal excitations. They show that at $\sigma = 0.0432\ \text{Å}^{-2}$ and for zero pressure, the superfluid-normal fluid transitions occurs at $T=0.72\pm0.02$ K. A recent article[22] describes the results of path-integral Monte Carlo calculations on a second layer of ^{4}He adsorbed on a flat structure modeling graphite. The authors model the first layer of helium atoms as a frozen hexagonal-packed structure. They show the boundaries of the phase diagram at low temperatures, indicating the phase transitions in the solid region, but neglecting the description of how the phase diagram evolves as the temperature increases.

Here, we present a set of PIMC calculations at $T \leqslant 1.5$ K and $\sigma < 0.094\ \text{Å}^{-2}$, to determine the equilibrium regions of the 2D solid, liquid, and gas and their coexistence regions.

METHOD

The PIMC method is a method which can calculate quantum properties by mapping the quantum system onto an equivalent classical model. The basic idea is to expand the density matrix

$$\rho(R,R';\beta) = \langle R | \exp(-\beta H) | R' \rangle \tag{1}$$

into a path integral

$$\rho(R,R';\beta) = \int \rho(R,R_1;\tau)\rho(R_1,R_2;\tau)\ldots\rho(R_{N-1},R';\tau) \times dR dR_1 dR_2 dR_{N-1} dR', \tag{2}$$

TABLE I. Energy versus coverage and temperature in the fluid phase. All calculations were done in a square periodic cell containing 30 atoms.

σ (Å^{-2})	$T=0.25$ K	$T=0.5$ K	$T=0.75$ K	$T=1$ K	$T=1.25$ K	$T=1.5$ K
0.0761	1.009±0.010	1.003±0.008	1.015±0.008	1.038±0.008	1.074±0.013	1.077±0.010
0.0677	0.089±0.012	0.126±0.014	0.143±0.016	0.187±0.026	0.287±0.031	0.433±0.014
0.0592	−0.577±0.012	−0.559±0.014	−0.552±0.016	−0.414±0.026	−0.234±0.031	−0.004±0.014
0.0508	−0.853±0.009	−0.859±0.016	−0.806±0.017	−0.668±0.027	−0.379±0.021	−0.084±0.012
0.0423	−0.919±0.010	−0.887±0.010	−0.789±0.019	−0.541±0.022	−0.235±0.021	0.043±0.011
0.0338	−0.816±0.013	−0.752±0.011	−0.554±0.022	−0.330±0.022	−0.030±0.015	0.268±0.010
0.0254	−0.611±0.015	−0.522±0.013	−0.272±0.016	−0.060±0.012	0.217±0.012	0.529±0.010
0.0169	−0.475±0.011	−0.360±0.014	−0.046±0.013	0.233±0.010	0.486±0.009	0.771±0.009
0.0085	−0.287±0.025	−0.088±0.025	0.225±0.016	0.539±0.015	0.839±0.018	1.134±0.009

where several complete sets of 2D coordinates ($R_1, \ldots, R_{N-1}$) have been introduced. Each of these R's represent the positions of all the particles in the system, in such a manner that each particle is described by $N+1$ coordinates forming a *path.* The additional degree of freedom takes into account the quantum fluctuations. In Eqs. (1) and (2), β is the inverse temperature ($\beta=1/k_BT$), while $\tau=\beta/N$. N is the number of additional coordinates introduced (also called *time slices*) and H is the system hamiltonian. The Bose statistics are accounted for by symmetrization of the density matrix:

$$\rho_{\mathrm{Bose}}(R,R';\beta)=\frac{1}{M!}\sum_P \rho(R,PR;\beta). \tag{3}$$

M is the number of atoms, and P is a permutation of particle labels $1,2 \ldots, M$. The average of any observable O, defined by

$$O=\langle R|O\ \exp(-\beta H)|R'\rangle, \tag{4}$$

can be found by expanding in a similar way. Additional details about the method are given elsewhere.[24]

Our aim in the present work is to calculate the boundaries and coexistence regions of the different phases of a pure 2D ^{4}He film: solid, normal liquid, superfluid, and gas. (We do not allow for the possibility of a hexatic phase, and cannot distinguish between commensurate and incommensurate solids, because we do not include a substrate.) We employed the canonical ensemble, i.e., in each simulation we kept fixed the temperature T, the number of particles M, and the dimensions of the simulation cell. The temperature was set between 0.25 and 1.5 K, with calculations every 0.25 K (with an additional set of points at 0.87 K), and the densities were taken in the interval $0<\sigma<0.094$ Å^{-2}. Most simulations contained 30 atoms. The coverage was varied by changing the cell size. Two types of cell were used: a square simulation cell, and a rectangular cell corresponding to a triangular solid at intermediate and high coverages ($\sigma>0.05$ Å^{-2}). The time step τ was fixed for all simulations at 0.025 K^{-1}, tests showing that this is sufficient for the range of densities considered. We used the Aziz[25] potential for the interaction between the helium atoms. To determine the finite-size effects in our calculations, we made two sets of simulations at $T=1.0$ and 0.87 K with 100 atoms and densities around the critical point, finding very small differences with the results for fewer atoms.

RESULTS

In Tables I and II we show the calculated energies. Table I indicates some results for the total energy and their dependence on the temperature and density when we use a square cell (''liquid''), while in Table II we can see the same, but for a rectangular cell (''solid''). The energy per atom and pressure were used to determine the free energy and thereby the phase lines as we discuss below.

Figure 1 is a summary of how the phase depends on temperature and coverage. In general terms, we can say that there exists a liquid-gas coexistence for densities between 0 and 0.044 Å^{-2} for temperatures below 0.87 K. The location of the boundaries is very similar to the experimental ones, although there are several noticeable differences (see below). For this coverage range and at higher temperatures the stable phase is the normal 2D fluid. For greater densities (0.044 Å^{-2} $<\sigma<$0.068 Å^{-2}) the ground state is a superfluid, with the transition to a normal fluid located in the temperature range from 0.72 to 0.90 K. Above the critical temperature,

TABLE II. Energy versus coverage and temperature for the triangular solid. All calculations were done with 30 atoms in a rectangular cell consistent with the solid symmetry.

σ (Å^{-2})	$T=0.25$ K	$T=0.5$ K	$T=0.75$ K	$T=1$ K	$T=1.25$ K	$T=1.5$ K
0.0931	4.86±0.04	4.88±0.03	4.94±0.05	5.00±0.04	4.95±0.04	4.95±0.05
0.0846	2.45±0.05	2.47±0.03	2.50±0.05	2.48±0.03	2.45±0.03	2.50±0.03
0.0761	0.98±0.03	1.01±0.04	1.00±0.03	1.01±0.03	1.02±0.03	1.02±0.02
0.0677	0.08±0.03	0.13±0.02	0.10±0.03	0.18±0.03	0.27±0.03	0.46±0.02
0.0592	−0.33±0.02	−0.33±0.03	−0.22±0.02	−0.14±0.02	−0.06±0.02	0.05±0.02
0.0508	−0.62±0.02	−0.56±0.02	−0.46±0.02	−0.32±0.02	−0.16±0.02	−0.04±0.02

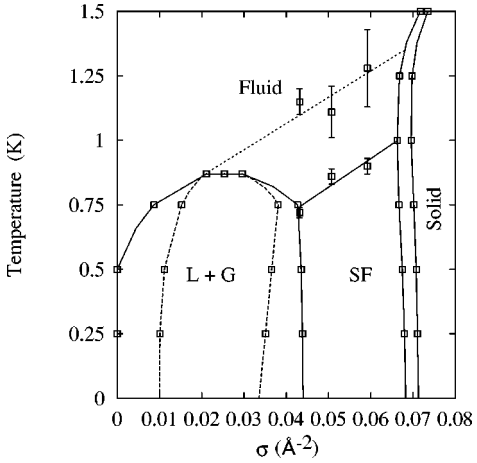

FIG. 1. Phase diagram for 2D ^{4}He as a function of coverage and temperature. The upper dotted line marks the loci of the maxima in the specific heat. The lower dashed line shows the spinodal line of the liquid-gas transition. The different phases are indicated by text or symbols ($L+G$, liquid+gas coexistence zone; SF, superfluid).

T_c, we see a line of maxima in the specific heat (line at $T \sim 1.15-1.30$ K in Fig. 1) as predicted by the Kosterlitz-Thouless theory.

If the helium coverage is greater than ~ 0.068 Å^{-2} (depending on the temperature), we observe a narrow coexistence zone region between the liquid and the triangular solid phase. The slope of the boundaries changes with temperature; when the boundary is with the superfluid phase, the slope is slightly negative, being positive in the zone of the normal fluid. This is because the superfluid has fewer excitations and hence lower entropy than the solid. At the highest temperature of this study (1.5 K), we observe a 2D solid for coverages greater than 0.073 Å^{-2}. Next we will discuss in detail the features of the calculated phase diagram and how the results were obtained.

In order to obtain the coexistence, we fit the calculated energy and pressure to polynomials. For this purpose we partitioned our runs into gas, liquid, and solid and chose appropriate forms for each phase.

We consider as ''solid'' all the structures calculated by using the rectangular lattice and whose structure factors, $S(k)$, are greater than 4. This means a coverage range $0.0677 \leqslant \sigma \leqslant 0.0931$ Å^{-2}. Conversely, we defined as ''liquid'' the structures obtained with the square simulation cell with $S(k)<2$ and whose densities are in the limit or outside the $L+G$ coexistence region, i.e., coverages in the interval $0.0423 \leqslant \sigma \leqslant 0.0592$ Å^{-2}. We obtained the free energies in both ''phases'' by fitting the energies *and* pressures to a polynomial in both coverage and temperature. The assumed expression for the free energy is

$$F(\sigma,T)=\sum_{i=0}^{m}\sum_{j=0}^{n} b_{ij}\sigma^i T^j. \tag{5}$$

Then, we can write the energy per He atom and the pressure as

$$E(\sigma,T)=-\sum_{i=0}^{m}\sum_{j=0}^{n} (j-1)b_{ij}\sigma^i T^j, \tag{6}$$

TABLE III. Coefficients of the least-squares fit of the total energy per He atom and pressure.

	Square	Rectangular	Gas
Number of points	22	24	8
χ^2/ν	1.24	1.61	0.33
b_{00}	-1.65	-1.82×10^{1}	
b_{03}	6.49	2.62×10^{1}	
b_{04}	4.61	-3.51×10^{1}	
b_{05}	-7.94	1.81×10^{1}	
b_{10}	9.35×10^{1}	8.35×10^{2}	1.74×10^{5}
b_{11}			-8.36×10^{5}
b_{12}			1.59×10^{6}
b_{13}	-3.81×10^{2}	-1.13×10^{3}	-1.48×10^{6}
b_{14}	-1.33×10^{2}	1.61×10^{3}	6.93×10^{5}
b_{15}	3.87×10^{2}	-7.96×10^{2}	-1.27×10^{5}
b_{20}	-3.11×10^{3}	-1.37×10^{4}	-2.05×10^{7}
b_{21}			9.82×10^{7}
b_{22}			-1.86×10^{8}
b_{23}	6.94×10^{3}	1.61×10^{3}	1.75×10^{8}
b_{24}	1.54×10^{3}	-2.37×10^{4}	-8.15×10^{7}
b_{25}	-6.71×10^{3}	1.14×10^{4}	1.50×10^{7}
b_{30}	3.10×10^{4}	8.03×10^{4}	
b_{33}	-4.07×10^{4}	-7.22×10^{4}	
b_{34}	-7.51×10^{3}	1.11×10^{5}	
b_{35}	-3.99×10^{4}	-5.31×10^{4}	

$$p(\sigma,T)=\sum_{i=1}^{m}\sum_{j=0}^{n} i b_{ij}\sigma^{i+1}T^j. \tag{7}$$

We use our simulation data to fit *simultaneously* the values of the total energy and the pressure (obtained from the virial relation) to obtain the b_{ij} coefficients. Using both constraints the fit is much better. The excitation spectra implies that at low temperature $E-E_0 \propto T^3$; thus we set $b_{i1}=b_{i2}=0$ for all i. We used the same values of m and n in the ''solid'' and ''liquid'' cases: $m=3$ and $n=5$ as was done at previous zero-temperature[17,18] calculations. That allows reasonable values of χ^2 for both series of fits, as can be seen in Table III. For the purposes of calculating the specific heat, we also fit the energies below 2.5 K to a similar expression to that of Ref. 1, i.e., a (5,4) Padé with a low-temperature limit as above.

In the gas phase (coverages lower than 0.010 Å^{-2}) we assumed a virial form for the free energy, expanding in powers of coverage and inverse temperature:

$$F(\sigma,T)=T\ln\left[\frac{2\pi\hbar^2\sigma}{m_{\mathrm{He}}Te}\right]+\sum_{i=1}^{2}\sum_{j=1}^{n'} b_{ij}\sigma^i T^{1-j}, \tag{8}$$

with $n'=5$ and m_{He} the mass of the ^{4}He atom. The first term of the right-hand side is the free energy for a 2D ideal gas.[23] The fitting coefficients are shown in Table III.

Liquid-gas coexistence zone

Figure 2 shows the pressure versus coverage for the seven temperatures for which we carried out simulations (0.25–1.5 K). In this density range we verified that we do not have a

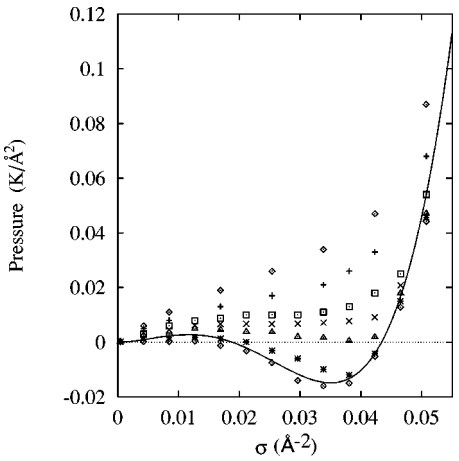

FIG. 2. Coverage dependence of the pressure (in K/Å^{-2}) in the fluid density range. Diamonds indicate the results for 1.5 K, and from there on, the symbols display at the data for all temperatures, ending at 0.25 K (stars). The line shows the results of Giorgini *et al.* using a DMC at zero temperature (Ref. 17).

solid phase by examining the structure factors as shown in Fig. 3. A structure factor corresponding to a solid has one or several isolated peaks with $S(k)>4$. In the upper part of Fig. 3, we show one such result at a temperature of 0.75 K and a density of 0.0761 Å^{-2}, well inside the solid region, as we can see in Fig. 1. In Fig. 3 we show two other structure factors at the same temperature. The diagram in Fig. 1 indicates that this temperature is the only one in our study in which we have three different phases: 2D gas, liquid, and solid. For higher temperatures, there is not a distinction between a liquid and a gas, and for lower ones, the gas has an inconveniently low coverage. We can observe striking differences in the $S(k)$'s: instead of a sharp peak, a 2D liquid presents a round maximum for a reciprocal vector corresponding approximately to the first-neighbor distance. There is also a difference between a liquidlike and a gaslike structure factor. In a gas, we have that $S(k)$ becomes practically constant for $k>1$ Å^{-1}, and that $S(0)$ is much greater than in the liquid case. If instead of a pure liquid or gas phase, we

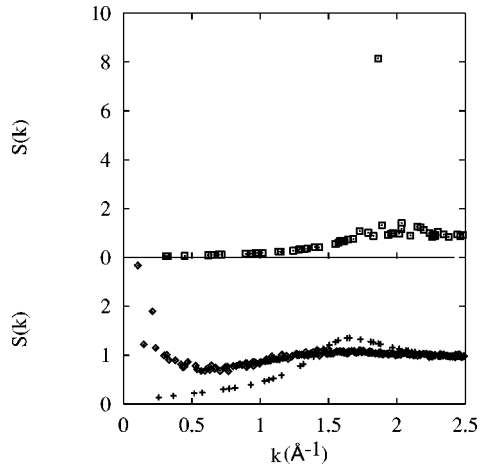

FIG. 3. Structure factors, $S(k)$ of three different phases at 0.75 K. Squares represent the structure factor for a solid (σ=0.0761 Å^{-2}). Crosses show the values for a liquid $S(k)$ (σ=0.0508 Å^{-2}) and diamonds are the data for a gas phase (σ=0.0085 Å^{-2}).

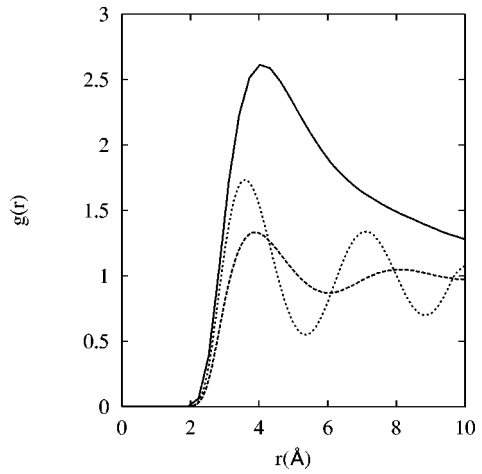

FIG. 4. Radial distribution functions for the same coverages shown in Fig. 3. Solid line, gas; dashed line, liquid; dotted line, solid.

are in the two-phase region zone or above the critical point, we have a mixture of the features of the pure liquid and gas structure factors.

The same information can be obtained by looking at the radial distribution functions, $g(r)$'s, but in a less quantitative way. In Fig. 4, we can observe that a gas radial distribution function (solid line) shows only a maximum, and that, quite reasonably, the number of maxima and their height increases in the liquid $g(r)$ (dashed line) and, over all, in the solid one (dotted curve). However, there is not a clear difference among the radial distribution functions for the three cases, as there is for the structure factors.

The behavior of the pressure isotherms can be divided into three groups. For $T>1$ K the pressure is a monotonically increasing function of the coverage. However, the isotherm at $T=$ 0.87 K is different; there is a flat zone between the densities 0.0338 and 0.0169 Å^{-2}. That means that there is a region ($\sigma\sim 0.02-0.03$ Å^{-2}) in which the second derivative of the pressure with respect to coverage ($d^2p/d\sigma^2$) is zero. This implies that $T=0.87$ K is the critical temperature for the liquid-gas phase transition. In accordance with that, for $T<0.87$ K, (0.75, 0.5, and 0.25 K), the pressure isotherms show instability zones (where $dp/d\sigma<0$), that correspond to a two-phase coexistence region, and whose range in σ increases as the temperature decreases.

To determine the limits of the liquid-gas coexistence zone, we matched the chemical potential of the liquid and gas phases. For constant number of particles and temperature, this implies

$$\int_{A_G}^{A_L} p\,dA = \int_{\sigma_G}^{\sigma_L} \frac{-p}{\sigma^2}\,d\sigma = 0, \tag{9}$$

where σ_G and σ_L are the equilibrium coverages of the gas and liquid phases, respectively (A_G and A_L stand for the corresponding areas) and p is the pressure. To carry out the necessary integrations, we fit the isotherms to three different polynomials (one for each temperature below 0.87 K). Using the fits, we calculate the equilibrium densities σ_G and σ_L. We also used them to obtain the spinodal curve defined by $(dp/d\sigma)=0$. This is the limit of metastability of the given

TABLE IV. Coexistence and spinodal coverages for three temperatures below the critical temperature for the liquid-gas phase transition. All values are in $Å^{-2}$ and the uncertainty for all of them is 0.002 $Å^{-2}$. G and L stand for gas and liquid phases and s_G and s_L for the low and high coverages of the spinodal curve. Also shown is the equilibrium pressure (in $K/Å^2$, its error bars are $\pm 0.0001 K/Å^2$).

T (K)	σ_G	σ_L	σ_{sG}	σ_{sL}	P
0.25	0.0	0.044	0.010	0.035	0.0001
0.50	0.0	0.044	0.011	0.037	0.0001
0.75	0.009	0.043	0.015	0.038	0.0040

phase. The equilibrium and spinodal coverages are given in Table IV and displayed in Fig. 1.

If we compare those results with the experimental data given in Refs. 2 and 4 for a second layer of helium in graphite, we can say that our coverage limits for the liquid-gas coexistence zone are very similar to the measurements at low temperatures. However, the calculated critical temperature ($T \sim 0.87$ K) is different from the experimental one ($T \sim 0.75$ K). On the other hand, the data of ^{4}He on top of molecular hydrogen[5] finds a critical temperature identical to that obtained in our simulations ($T \sim 0.87$ K). In addition, Ref. 10 reports a slightly greater T_c for a third layer of helium adsorbed on graphite. Our results are strictly correct only for a mathematically two-dimensional ^{4}He film. This is a good model for some but not all real substrates.

Figure 2 also displays the isotherm at $T=0$ K obtained in the DMC calculations by Giorgini *et al.*[18] We observe that their data is very similar to the results for our lower temperature isotherm ($T=0.25$ K), even if the potential is slightly different. Moreover, if we compare the energies at the minimum of the energy curves in both models, we obtain comparable values; -0.919 K versus -0.89706 of Ref. 18, a discrepancy of about 2%.

Solid-liquid coexistence

To calculate the solid-liquid phase line, we estimated the free energies per He atom and performed the ''double tangent construction'' between the two phases. The slope of the tangent is the equilibrium pressure. In Fig. 5, we display both the free energy and the tangent line for a temperature of 1 K (lines). The symbols represent the values of the total energy per atom in the rectangular (solid, diamonds) and square (liquid, pluses) simulation cells. As we can see, at $T=1$ K, the total energy is slightly higher than the free energy because of the entropy. That difference increases with temperature, in such a manner that at $T=0.25$ K, free and total energy are nearly identical, being appreciably different at $T=1.5$ K.

The limits of the solid-liquid coexistence zone for all temperatures are given in Table V (and displayed in Fig. 1). As we can see, the two-phase zone is rather narrow, which means there is a solid phase in a range of coverages greater than ~ 0.07 $Å^{-2}$. That limit would be low enough to allow the existence of a stable solid before the completion of the second and third layers of helium on graphite (0.08 and 0.076 $Å^{-2}$, respectively). However, while for the second layer there are experimental data that support the existence of a solid phase at high coverages (or at least of a solid-liquid coexistence),[2,4] for third and successive layers there is no such evidence.[10] The likely explanation is that one cannot ignore movement in the perpendicular direction for those higher layers. That limits the existence of the solid to the first few layers, unless the substrate has an unusually strong binding energy.

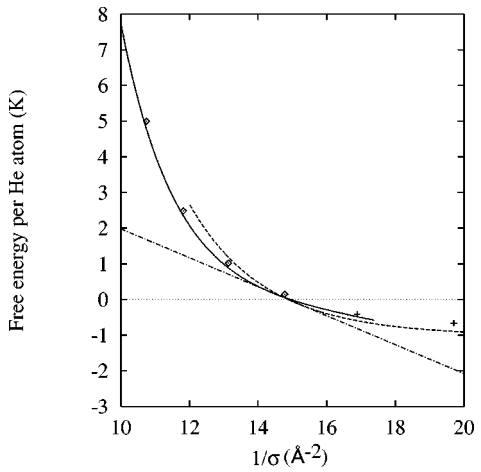

FIG. 5. Free energy versus the atomic area at 1 K. Symbols display the results of the total energy obtained in the simulations (diamonds, solid values; crosses, fluid). The solid and dashed lines are least-squares fits to the experimental data. The dashed-dotted line represents the common tangent line of the Maxwell construction.

Normal fluid-superfluid

The density range between the fluid-gas and solid-liquid two-phase regions is the stability range of the liquid. For $T \sim 0.72-0.90$ K, depending on the coverage, we found a superfluid, while for higher temperatures and densities lower than 0.06 $Å^{-2}$, we have a normal liquid. We define a superfluid phase by a nonzero superfluid fraction (not by momentum condensation, since that only exists in 2D in the ground state.) The fraction of helium atoms in the superfluid phase can be estimated from the mean squared winding number.[24] The winding number is the flux of paths around the periodic boundary conditions of the simulation cell.

However, size effects smear out the transition between the normal fluid and the superfluid (see Fig. 6). To determine the critical temperature, we used the following relations from the Kosterlitz-Thouless theory:[16,1]

TABLE V. Coexistence coverages for solid-liquid (S-L) transition in $Å^{-2}$. The error bars are 0.0010 $Å^{-2}$. Also shown is the equilibrium pressure.

T (K)	σ_L	σ_S	p ($K/Å^2$)
0.25	0.0680	0.0711	0.466
0.50	0.0675	0.0708	0.449
0.75	0.0667	0.0702	0.418
1.00	0.0663	0.0693	0.406
1.25	0.0668	0.0698	0.431
1.50	0.0717	0.0735	0.615

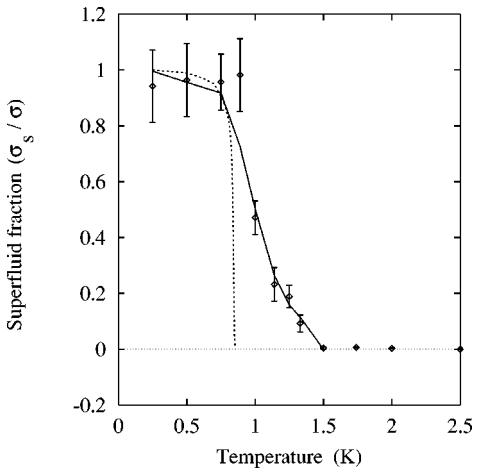

FIG. 6. Superfluid fraction versus temperature for a coverage $\sigma = 0.0508$ Å^{-2}. The diamonds are the simulation results, while the solid line is the result of a least-squares fitting procedure (see text). The dotted line is the result of the application of the Kosterlitz-Thouless theory to a system with the same parameters, in the limit of infinite area.

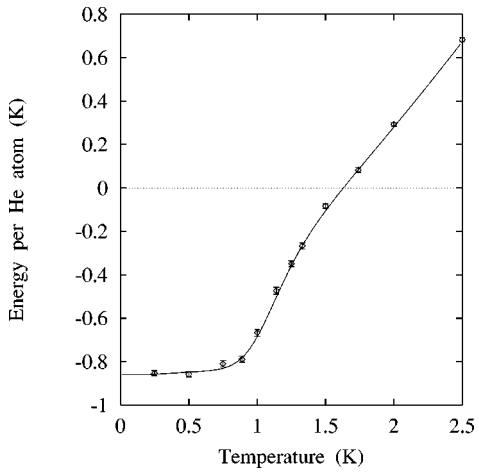

FIG. 7. Temperature dependence of the energy for the same coverage shown in Fig. 6. Diamonds are simulation results, and the line represents a least-squares fit.

$$\frac{dK^{-1}}{dl} = 4\pi^3 y^2(l), \tag{10}$$

$$\frac{y(l)}{dl} = [2 - \pi K(l)]y(l), \tag{11}$$

where

$$K(l) = \frac{\hbar^2 \sigma_s}{m k_B T} \tag{12}$$

with initial conditions

$$K(l=0) = \frac{\hbar^2 \sigma}{m k_B T} \tag{13}$$

$$y(l=0) = \exp(-\beta E_c). \tag{14}$$

The integration limits are from l equal to zero to $l = \ln[L/2d]$, with L being the size of the simulation cell. The two free parameters, E_c (''vortex core energy'') and d (''vortex core diameter'') are obtained by a least-squares fit to the simulation results.[1] We performed two sets of fits for coverages $\sigma = 0.0508$ Å^{-2} and $\sigma = 0.0592$ Å^{-2}. The third point displayed in Fig. 1 was taken from Ref. 1. The E_c and d's values obtained for the three coverages are given in Table VI. The critical temperature is then the temperature at which $\sigma_s = 0$ when $L \to \infty$. In Fig. 6 we show the temperature dependence of the σ_s/σ ratio for $\sigma = 0.0508$ Å^{-2}. The solid line corresponds to the least-squares fit, and the dotted one indicates the limit for $L \to \infty$ ($T_c = 0.86 \pm 0.02$ K).

TABLE VI. Equilibrium parameters E_c and d for the Kosterlitz-Thouless theory as obtained from a least-squares fit to the superfluid fraction. The critical temperature for superfluid phase transition is shown in the last column.

σ (Å^{-2})	$E_c(K)$	d (Å)	T_c
0.0432	2.7±0.2	3.7±0.4	0.72±0.02
0.0508	2.5±0.2	3.7±0.7	0.86±0.02
0.0592	2.4±0.1	4.6±0.3	0.90±0.03

In the Kosterlitz-Thouless transition there is also a maximum in the specific heat at temperatures above T_c. To determine the locus of those peaks shown in Fig. 1, we took the derivative (dE/dT) and took note of the temperature at which a maximum exists. The temperature dependence of the energy is shown in Fig. 7 for a coverage $\sigma = 0.0508$ Å^{-2}. In Fig. 8, we display the data for the specific heat for the same coverage. The solid line is the heat capacity determined by differentiating the (5,4) Padé we fit to the energy at this coverage. The dashed line are the results of Greywall[4] with a coverage of 0.1700 Å^{-2} (full monolayer of He on graphite $+ \sigma_2 = 0.05$ Å^{-2} on the second layer). The maximum of the experimental specific heat is located at a temperature slightly lower than the one obtained in our simulations. That probably could be attributed to the movement of the atoms in the

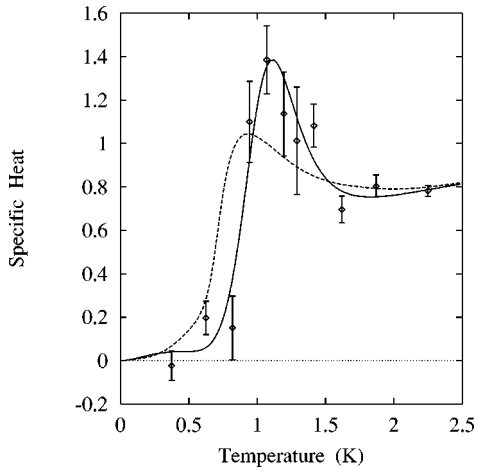

FIG. 8. Specific heat versus temperature for $\sigma = 0.0508$ Å^{-2}. The symbols correspond to the numerical derivative of the simulation data given in Fig. 7, and the line is the derivative of the (5,4) Padé used as a fit. The dashed line shows the experimental results of Greywall (Ref. 4) at a second layer coverage of 0.05 Å^{-2}.

z direction,[14,21] not taken into account here, since the contribution due to the first layer has been subtracted[4] out.

The line of maxima was extended to join the critical point ($T \sim 0.87$ K). This line, together with the lower coverage $L+G$ coexistence zone, produces a boundary with a shape very similar to that in experimental phase diagrams obtained by heat-capacity experiments.[4,2] However, our results indicate that part of that boundary is not a coexistence zone, but the stability zone of a superfluid. Thus, the experimental line can be interpreted as the signature of the Kosterlitz-Thouless transition.

Once again, those results are compatible with the experimental data of Crowell and Reppy.[8,10] By means of torsional oscillator experiments they found that for a second layer of helium on graphite, the coverage interval for a superfluid was between ~ 0.05 and 0.07 Å^{-2} (for temperatures lower than 0.75 K). The upper limit is very similar to the lower boundary of the solid-liquid coexistence region as it appears in our data. However, between the coverage at which our simulations (and those of Refs. 17,18) predict a self-bound fluid (0.044 Å^{-2}) and the lower limit given above there is a discrepancy worth mentioning. That difference was attributed to the existence of ''patches'' of liquid due to the substrate inhomogeneity.[10,26] One can see that to get a superfluid it is necessary to have a network of connecting patches, which may not be possible until greater coverages than 0.044 Å^{-2}. On the other hand, for the third layer, they found superfluidity near the beginning of layer completion. This may be due to multilayer effects not considered here, or to percolation between superfluid ''patches.''

p-T representation of the phase diagram

In Fig. 9 we display the same phase diagram in Fig. 1, but this time in the pressure versus temperature plane. The symbols represent the simulation results, while the lines are guides-to-the-eye. The three crosses located in the lower right part of the figure indicate the location of the maxima of the specific heat given in Fig. 1, and therefore, they do not signal a phase change. The solid square indicates the position of the critical point.

We observe that as in the bulk ^{4}He, there is no triple point between the solid, liquid, and gas phases. There are, however, two other triple points. One of them is among the gas, normal fluid, and superfluid phases at around 0.72 K, and the other between the two fluids and the solid region. The shape of the boundary of the stability zone of the solid

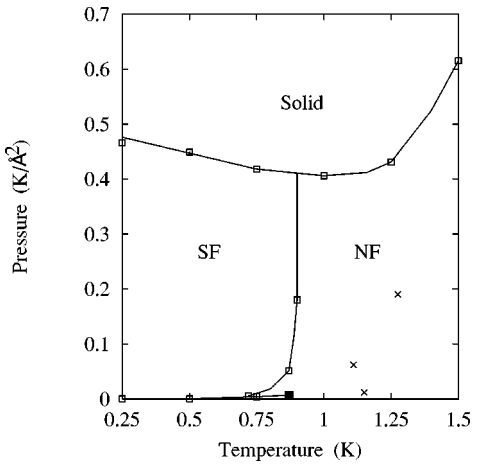

FIG. 9. Phase diagram as a function of pressure and temperature. The crosses mark the locus of the maxima in the specific heat given in Fig. 1, (they are not phase lines). The black square is the critical point.

permits, in some region of pressures, to liquefy a solid by reducing the temperature. In this, the behavior of the 2D phase diagram is similar to its 3D counterpart.

SUMMARY

We have calculated with path-integral Monte Carlo the energy of a 2D ^{4}He film for temperatures lower than 1.5 K and coverages in the range $0 < \sigma < 0.094$ Å^{-2}. Our results are similar to those obtained with $T=0$ methods,[20,21,17,18] but take into account the influence of thermal excitations over a range of helium densities. We use this information to determine the region of stability of the gas, normal fluid, superfluid, and solid. By comparison with the available experimental data, we can say that the *second* layer of ^{4}He adsorbed on graphite is well described by a 2D model. For an accurate description of the third and successive layers, the motion of the atoms in the z direction is important.

ACKNOWLEDGMENTS

We used the computational facilities at the NCSA. This research was supported by NSF DMR 94-224-96 and the Department of Physics at the University of Illinois. M.C.G. thanks the Spanish Ministry of Education and Culture for financial support.

[1] D. M. Ceperley and E. L. Pollock, Phys. Rev. B **39**, 2084 (1989).
[2] S. E. Polanco and M. Bretz, Phys. Rev. B **17**, 151 (1978).
[3] D. S. Greywall and P. A. Busch, Phys. Rev. Lett. **67**, 3535 (1991).
[4] D. S. Greywall, Phys. Rev. B **47**, 309 (1993).
[5] P. S. Ebey and O. E. Vilches, J. Low Temp. Phys. **101**, 469 (1995).
[6] R. C. Ramos, Jr., P. S. Ebey, and O. E. Vilches, J. Low Temp. Phys. **110**, 615 (1998).
[7] D. J. Bishop, J. E. Berthold, J. M. Parpia, and J. D. Reppy, Phys. Rev. B **24**, 5047 (1981).
[8] P. A. Crowell and J. D. Reppy, Phys. Rev. Lett. **70**, 3291 (1993).
[9] P. A. Crowell and J. D. Reppy, Physica B **197**, 269 (1994).
[10] P. A. Crowell and J. D. Reppy, Phys. Rev. B **53**, 2701 (1996).
[11] J. Nyèki, R. Ray, V. Maidanov, M. Siqueira, B. Cowan, and J. Saunders, J. Low Temp. Phys. **101**, 279 (1995).
[12] J. Nyèki, R. Ray, G. Sheshin, V. Maidanov, V. Mikheev, B. Cowan, and J. Saunders, Fiz. Nizk. Temp. **23**, 515 (1997).
[13] G. Zimmerli, G. Mistura, and M. H. W. Chan, Phys. Rev. Lett. **68**, 60 (1992).
[14] W. M. Saslow, G. Agnolet, C. E. Campbell, B. E. Clements, and

E. Krotscheck, Phys. Rev. B **54**, 6532 (1996); C. E. Campbell, B. E. Clements, E. Krotschek, and M. Saarela, *ibid.* **55**, 3769 (1997).
[15] P. J. Shirron and J. M. Mochel, Phys. Rev. Lett. **67**, 1118 (1991).
[16] G. Agnolet, D. F. McQueeney, and J. D. Reppy, Phys. Rev. B **39**, 8934 (1989).
[17] P. A. Whitlock, G. V. Chester, and M. H. Kalos, Phys. Rev. B **38**, 2418 (1988).
[18] S. Giorgini, J. Boronat, and J. Casulleras, Phys. Rev. B **54**, 6099 (1996).
[19] C. Um, J. Kahng, Y. Kim, T. F. George, and L. N. Pandey, J. Low Temp. Phys. **107**, 283 (1997).
[20] B. E. Clements, J. L. Epstein, E. Krotscheck, and M. Saarela, Phys. Rev. B **48**, 7450 (1993).
[21] B. E. Clements, H. Forbert, E. Krotscheck, M. Saarela, and C. J. Tymczak, Phys. Rev. B **50**, 6958 (1994).
[22] M. Pierce and E. Manousakis, Phys. Rev. Lett. **81**, 156 (1998).
[23] L. D. Landau and E. M. Lifshitz, *Statistical Physics* (Pergamon, New York, 1980).
[24] D. M. Ceperley, Rev. Mod. Phys. **67**, 279 (1995).
[25] R. A. Aziz, A. R. Janzen, and M. R. Moldover, Phys. Rev. Lett. **74**, 1586 (1995).
[26] J. G. Dash, Phys. Rev. Lett. **41**, 1178 (1978).